π-Loops With ds Josephson Junctions

M. I. Faley, P. Reith, V. S. Stolyarov, I. A. Golovchanskiy, A. A. Golubov, H. Hilgenkamp, and R. E. Dunin-Borkowski

***Abstract*—We fabricated Josephson junctions (JJs) between the d-wave superconductor (SC) $YBa_2Cu_3O_7$-x (YBCO) and the s-wave SC Nb (ds-JJs) on graphoepitaxially buffered MgO substrates, studied ds-JJs at temperatures down to 30 mK and employed these JJs in π-loops. Current-voltage characteristics of ds-JJs oriented along the [100] axis of YBCO exhibited up to a factor of 200 higher critical current densities than ds-JJs oriented along the [110] axis of YBCO. The critical current I_c and the I_cR_n product of [100]-oriented 3 μm wide ds-JJs are $\sim$70 μA and $\sim$200 μV, respectively, at 4.2 K. Rectangular arrays of up to 40 000 π-loops based on such ds-JJs were investigated using a low temperature scanning superconducting quantum interference device (SQUID) microscope. We observed ordering of spontaneously generated half integer magnetic flux quanta in the π-loops correlated with minute spurious background magnetic fields, as well as with configurations and mutual coupling of the π-loops. We manipulated the magnetic states of the π-loops by the local application of magnetic fields using nearby planar coils. This paper paves the way for the use of π-loops in computations that are based on annealing processes.**

***Index Terms*—High-temperature superconductors, Josephson junctions, superconducting quantum interference devices (SQUIDs), scanning probe microscopy, quantum computing.**

I. Introduction

HYBRID Josephson junctions between the d-wave superconductor (SC) $YBa_2Cu_3O_{7-x}$ (YBCO) and the s-wave SC Nb (ds-JJs) can be used for the realization of π-loops, π-superconducting quantum interference devices (SQUIDs) and quiet qubits and for the self-biasing of data storage cells in rapid single flux quantum (RSFQ) circuits [1]–[5]. The application of π-phase shifters based on ds-JJs can potentially improve the integration scale of superconducting logic circuits and may allow the use of multiple current lines to generate local high bias magnetic fields in nanoscale devices to be avoided. When compared with π-phase shifters that are based on ferromagnetic barriers [6], [7], ds-JJs are not magnetic and do not exhibit ferromagnetic hysteresis and noise. Moreover, low-energy quasiparticle dissipation resulting from nodal quasiparticles and zero energy bound states in these junctions is found to be weak [8].

These features of ds-JJs are favourable for their application in logic circuits and quantum computing. In the case of qubits, one can suppress decoherence effects due to nodal quasiparticles in YBCO using size quantization in sufficiently narrow ($<<1$ μm) YBCO electrodes [9]. However, the experimental verification of the applicability of ds-JJs for quantum computing is still lacking. Until now, ds-JJs were only fabricated on $SrTiO_3$ (STO) substrates. Thick YBCO structures may crack on STO due to the large difference in thermal expansion coefficient between YBCO and STO [10]. This problem can be avoided by using buffered single crystal MgO substrates, which are also much cheaper and readily available in larger sizes when compared to single crystal STO substrates.

The present paper contains new results on the fabrication of novel ds-JJs on graphoepitaxially buffered MgO substrates, the implementation of such ds-JJs in different designs of π-loops and the manipulation of the magnetic states of the π-loops by integrated bias flux loops using readout of the magnetic states by a low temperature scanning SQUID microscope (SSM) [11]–[13].

II. Experimental

The base electrodes of ramp type ds-JJs and π-loops were made out of 500 nm thick superconducting YBCO and 160 nm thick STO films deposited by high-oxygen-pressure sputtering [14], [15] on MgO substrates that were covered by an YBCO-STO graphoepitaxial buffer layer [16]. YBCO films of similar thickness that were deposited on STO substrates often revealed cracks and, in general, less reproducible electron transport properties.

Patterning of the base YBCO electrode was performed by Ar^+ ion milling through the entire film thickness to the MgO substrate with a rotating substrate at a 60° angle of incidence using a mask of AZ5214E photoresist that was melted for 30 min at 150 °C in order to round the edges. After ion milling, the rest of the photoresist was removed using acetone and an oxygen plasma, followed by the deposition of a 6 nm thick YBCO film. Deposition of the thin film of YBCO recovered the surface of the YBCO film by means of a final cleaning from organics,

Manuscript received October 30, 2018; accepted December 29, 2018. Date of publication January 10, 2019; date of current version February 1, 2019. This work was supported by the PGI-5 FZJ CEI E-Project (E.23102.76). The work of V. S. Stolyarov and I. A. Golovchanskiy was supported by the Russian Science Foundation under Project 18-72-10118. *(Corresponding author: Michael I. Faley.)*

M. I. Faley and R. E. Dunin-Borkowski are with the PGI-5 Forschungszentrum Jülich GmbH, 52428 Jülich, Germany (e-mail: m.faley@fz-juelich.de).

P. Reith, A. A. Golubov, and H. Hilgenkamp are with the Faculty of Science and Technology and the MESA+ Institute for Nanotechnology, University of Twente, Enschede 7500, The Netherlands (e-mail: p.reith@utwente.nl).

V. S. Stolyarov and A. A. Golubov are with the Moscow Institute of Physics and Technology, Dolgoprudny 141701, Russia (e-mail: vasiliy.stoliarov@gmail.com).

I. A. Golovchanskiy is with the Moscow Institute of Physics and Technology, Dolgoprudny 141701, Russia, and also with the National University of Science and Technology MISIS, Moscow 119049, Russia (e-mail: golov4anskiy@gmail.com).

Color versions of one or more of the figures in this paper are available online at http://ieeexplore.ieee.org.

Digital Object Identifier 10.1109/TASC.2019.2892078

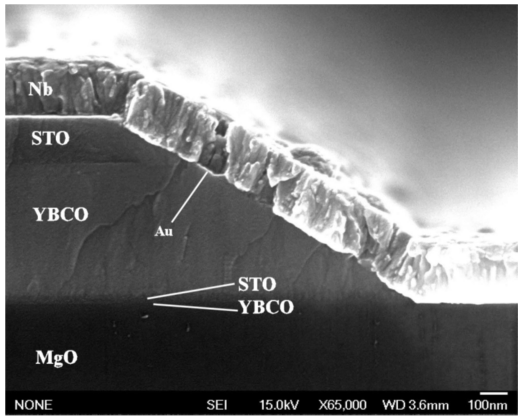

Fig. 1. SEM image of a ramp edge type ds-JJ. The image was obtained by using a cut of the sample perpendicular to the edge. The slope of the edge is about 30°.

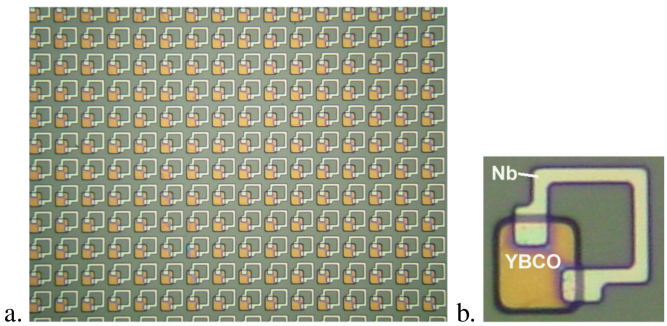

Fig. 2. (a) An optical microscope image showing part of an array of π-loops with 6 μm wide ds-JJs. The spatial period of the array is 28 μm in both directions. (b) Magnified view of a single loop with the components labeled. The Nb loop connects ds-JJs that were prepared along the [100] and [110] axes of a square island of YBCO film.

re-crystallization and re-oxygenation. In the next step, a 6 nm thick Au barrier layer and 200 nm thick Nb top electrodes were deposited using DC magnetron sputtering. The 3 μm or 6 μm wide perpendicularly oriented junctions of the top electrode were structured by Ar ion milling with a rotating substrate at a 10° angle of incidence using a mask of AZ nLOF2020 resist exposed by deep-UV with a 250 nm wavelength. A high-resolution scanning electron microscopy (SEM) image of a cross-section of a ds-JJ is shown in Fig. 1.

Ds-JJs along the [100] and [110] axes of YBCO were prepared and their current-voltage characteristics *I(V)* were measured at temperatures of 4.2 K, 1.43 K and 30 mK. Temperatures below 4.2 K can be used to achieve higher critical currents of the JJs and larger energy gaps in the superconducting circuits.

Arrays of up to 40000 π-loops were prepared, each with a side length of 16 μm, based on the ds-JJs (see Fig. 2a) and their magnetic states were measured using the SSM at 4.2 K. The inductance of an individual square π-loop of $\sim$23 pH (see Fig. 2b) was estimated using the software package 3D-MLSI [17]. The diameter of the pickup loop of the SQUID in the SSM is $\sim$3 μm and the SQUID-to-sample separation is $\sim$5 μm [13]. The spatial resolution of the SSM is $\sim$6 μm. The samples were covered with 2 μm thick AZ nLOF2020 photoresist to protect the devices from damage during scanning.

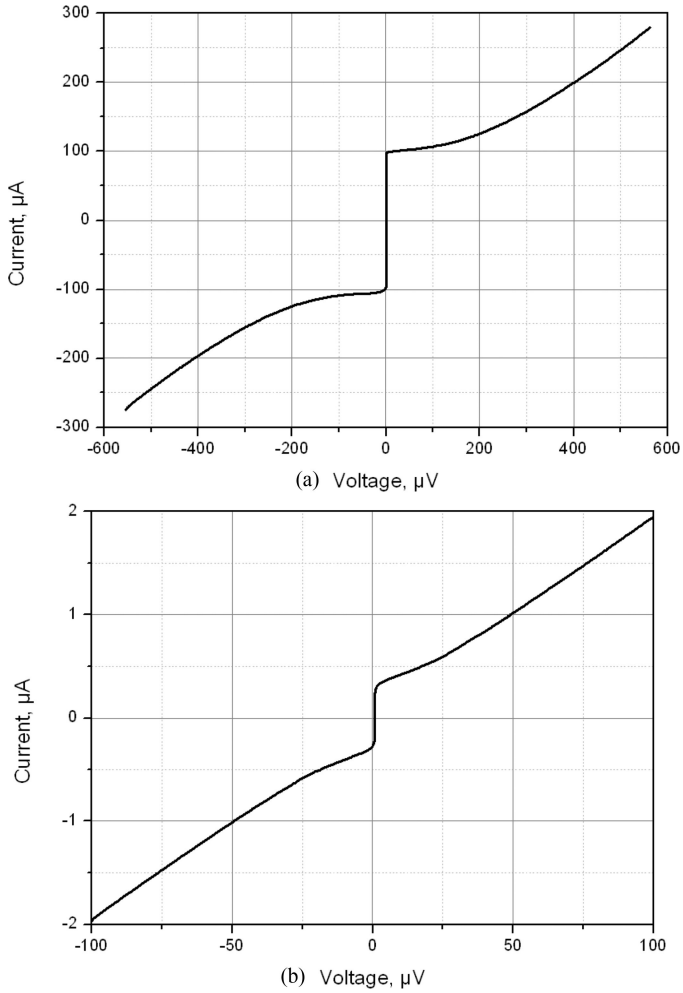

Fig. 3. I(V) characteristics of ds-JJ prepared (a) along the [100] axis of YBCO and (b) along the [110] axis of YBCO measured at 4.2 K.

III. Results

A. Measurements of I(V) and $I_c(T)$ Characteristics

Current-voltage *I(V)* characteristics of 3 μm wide ds-JJs oriented along the [100] axis of YBCO exhibited up to a factor of 200 higher critical current densities than similar ds-JJs oriented along the [110] axis of YBCO (see Fig. 3).

A spread of the critical currents of the ds-JJs $\delta I_c/I_c$ down to $\sim$15% was achieved. The dependence of the critical current I_c of the [100]-oriented ds-JJs increased monotonically with decreasing temperature (T) and saturated at T $<$ 2 K with values of $I_c(30\ \mathrm{mK}) \cong I_c(1.43\ \mathrm{K}) \cong 1.2 \times I_c(4.2\ \mathrm{K})$ expected for dirty weak links described by the Kulik–Omelyanchuk theory (see, e.g., a review [18]).

B. SSM Measurements of a π-Loop Array in Magnetic Fields

The π-loop array (see Fig. 2) was cooled to 4.2 K in a small ambient magnetic field of about 10 μT achieved by partial screening of the Earth's magnetic field with a μ-metal cylinder surrounding the liquid helium cryostat. Regular features of the magnetic flux distribution, identified as vortices, were clearly

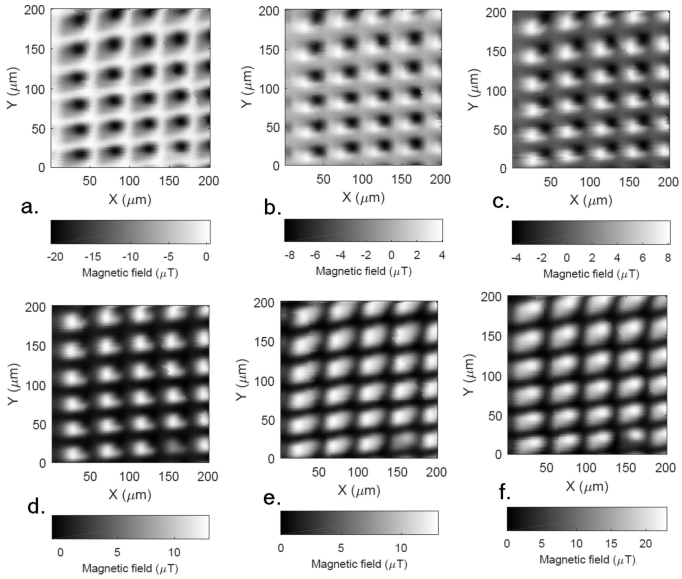

Fig. 4. Magnetic field images of the array of π-loops cooled to 4.2 K at various applied magnetic fields: (a) -30 μT, (b) -15 μT, (c) -10 μT, (d) -5 μT, (e) 10 μT, and (f) 30 μT.

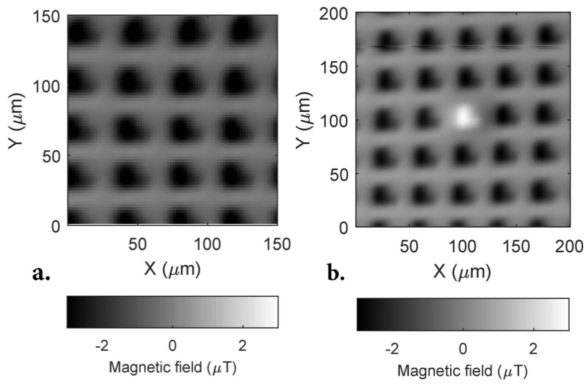

Fig. 5. Measurements with π-loops cooled to 4.2 K in a superconducting shield: (a) Part of the array in which all of the vortices are oriented in the same direction; (b) Part of the array with one oppositely directed vortex.

observed using SSM. The vortices were arranged in a square lattice with a spatial period of 28 μm in both directions, which corresponds to the spatial period of the π-loop array.

Next, we varied the external magnetic field between -30 μT and $+30$ μT (see Fig. 4). Clear changes are visible in the direction and amplitude of the stray field of the vortices. One loop near the bottom right shows a different behavior in some scans. This may indicate that this particular loop is damaged or dirty. The images at -15 μT and -10 μT seem to show some sort of dipolar behavior, which may be due to comparable values of the induced and background magnetic fields.

Further measurements were performed with the sample surrounded by a superconducting Nb shield to reduce the background fields to $<<1$ μT. The samples were cooled with a magnetic shield to reduce environmental influences. An initial scan over the 200×200 μm^2 area (Fig. 5) showed vortices that are spontaneously induced in the loops. The array structure is

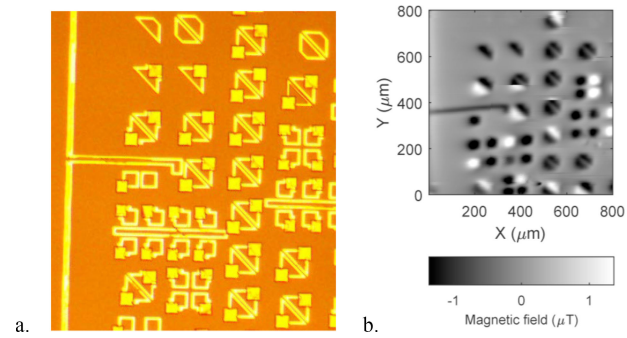

Fig. 6. (a) Optical microscope image of the sample area scanned with SSM. (b) SSM scan of the sample.

clearly visible, and all vortices with few exceptions (see Fig. 5a and Fig. 5b) are oriented in the same direction.

A rough analysis of the SQUID voltage range measured indicated that the total magnetic flux in each vortex was approximately half a flux quantum ($\Phi_0/2$). By integration of the data points attributed to one vortex surrounded by similarly directed vortices (Fig. 5a), we obtained a value of approximately $0.48\Phi_0$, which is close to the expected value of $\Phi_0/2$. The total measured magnetic flux of a single vortex surrounded by oppositely directed vortices (Fig. 5b) was approximately $0.42\Phi_0$. The expected screening parameter of these π-loops $\beta_L = 2\pi L I_c/\Phi_0 \cong 14$ for the 6 μm wide ds-JJs. The deviation of the observed magnetic fluxes in the vortices from the expected values can have various reasons:

a) Overlapping of stray fields: the vortices are densely packed, so the stray fields from neighbors will add/subtract from the field of a vortex of interest;
b) The data are offset by a fixed value to subtract background fields during analysis, but the background fields can vary over the scanned area;
c) Due to the finite distance of $\sim$2 μm between the π-loops and the SQUID, part of the magnetic flux passes by the SQUID and remains unmeasured, leading to a reduced measured value;
d) Phase decay $2\Delta\phi$ at the ds-JJs due to flow of the superconducting current $I_s = I_c \times \sin(\Delta\phi)$.

C. Measurements on Gradiometrically Coupled π-Loops

Two types of measurements on gradiometrically-coupled π-loops were performed in a superconducting shield: regular SSM measurements and local magnetometry. The former experiment was performed to determine the flux state in various configurations of the Nb and YBCO electrodes (pure Nb-loop, π-loop, etc.). Figs. 6a and 6b show the scanned area and an SSM image of the same area. All of the π-loops possess non-zero magnetic flux, while the Nb-only loops have zero flux: compare the optical and magnetic images of the first and fourth lines of the loops in Fig. 6a and 6b, respectively.

Some of the π-loops that have 3 μm wide ds-JJs change their flux direction during scanning, while the flux in the π-loops with 6 μm wide ds-JJs remains unchanged. This might be due to some interaction with the sensor, either mechanical or

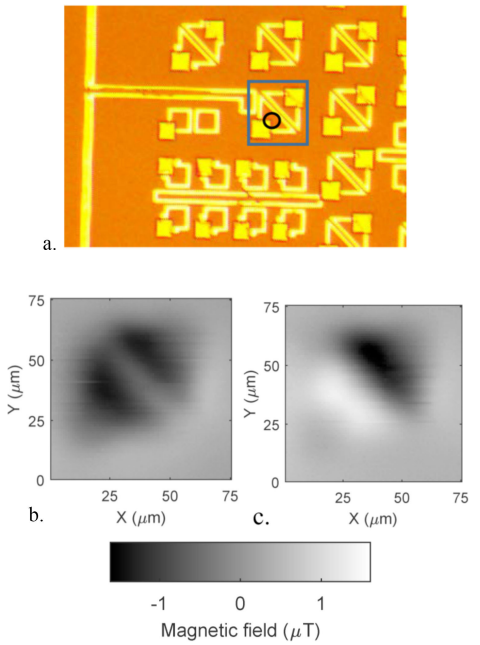

Fig. 7. (a) Optical microscope image of the sample area scanned with SSM. (b) and (c) SSM scans of the gradiometric π-loop in the two different states. The scale of magnetic fields in shades of grey is related to (b) and (c).

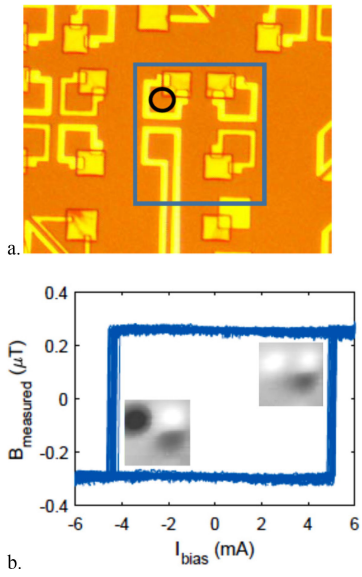

Fig. 8. (a) Optical microscope image of another part of the sample, with the location of the SQUID sensor (not to scale) circled. The scanned area for the insets in (b) is indicated by a rectangle. (b) Hysteresis loop of π-loop indicated by the circle in (a). The signal in the lower right corner of the insets is weaker because of the narrower Nb line in this loop.

electromagnetic. It shows that the energy barrier for switching of π-loops based on 3 μm wide ds-JJs is low relative to the energy barrier for switching of π-loops based on 6 μm wide ds-JJs. The absolute values of the spontaneous fluxes do not show a dependence on the widths of the ds-JJs in the investigated π-loops. Note that some pairs of loops have antiparallel fluxes, as expected from their antiferromagnetic mutual interaction. The fact that some loop pairs have parallel flux indicates that the interaction between two loops is small.

D. Switching of Flux in π-Loops Using Local Flux Bias Lines

During the SSM scan, a current of 20 μA was applied to the bias line. This makes it visible during SSM, which is useful for two reasons: it allows the integrity of the bias lines to be verified (i.e., no damage, shorts, etc.) and it can be used as a landmark to orient ourselves on the sample.

SSM scans were also performed to observe flux states after applying different currents to the bias line. Local magnetometry was carried out to see the change in flux state while ramping the current. The sensor was placed above a loop near the bias line and the current through the bias line was varied while the SQUID response was measured. This allowed the real-time observation of flux states flipping under the bias line field. By performing small scale scans, the sensor was placed above a specific loop near the bias line. The sensor was placed at a local maximum of the flux response, which should coincide with the 'center' of a (half) flux quantum. The current through the bias line varied and the SQUID response was recorded.

After testing, the current in the bias line was swept repeatedly in the sequence $0 \rightarrow I_{\max} \rightarrow I_{\min} \rightarrow 0$. In this case, we swept between -1.5 and $+1.5$ mA, with a rate of 50 μA/s. The SQUID voltage was recorded and later converted to magnetic field values.

As the magnetic field of the flux bias line is ramped up, the diamagnetic screening current in the π-loop expels the flux from the loop until the critical current $I_c(T)$ at this temperature is reached and the flux in the ring changes abruptly. These abrupt changes were identified by clear jumps in the SQUID voltage. These jumps are located around 0.5 mA and -0.8 mA for the gradiometric $\pi-$loop with 3 μm wide ds-JJs shown in Fig. 7 and they are located around 5 mA and -4.5 mA for the π-loop with 6 μm wide ds-JJs shown in Fig. 8. We therefore note that the flux state in the π-loop can be adjusted using the bias line. In addition, a slightly preferred orientation is indicated by the observed asymmetry in the threshold values of the bias current. In our case, the 'up' state is preferred. This can be attributed to the antiferromagnetic (dipole) influence of the second loop in the pair, which is in the 'down' state at all times (see insets in Fig. 8b). Higher half integer magnetic flux quanta states in the π-loop ($3/2\Phi_0$, $5/2\Phi_0$, etc.) were observed at higher currents in the flux bias line.

The exact point of switching varies slightly for every loop. This could be due to a small amount of thermal energy causing the switch when the energy barrier becomes low enough because of the applied field.

IV. Conclusion

We prepared ds-JJs between the d-wave YBCO and s-wave Nb superconducting films on graphoepitaxially buffered MgO substrates, studied ds-JJs at temperatures down to 30 mK and

used these JJs in π-loops. The use of graphoepitaxially buffered MgO substrates improved the reproducibility and reliability of ds-JJs with a 500 nm thick YBCO layer. Current-voltage characteristics of ds-JJs oriented along the [100] axis of YBCO exhibited up to 200 times higher critical current densities than ds-JJs oriented along the [110] axis of YBCO. A strong dependence of I_c on the orientation of the ds-JJs and their moderate temperature dependence are in agreement with theoretical expectations.

Rectangular arrays of up to 40000 π-loops based on such ds-JJs were investigated using a low temperature SSM. We observed ordering of the spontaneously generated $\Phi_0/2$ magnetic flux in the π-loops correlated with minute spurious background magnetic fields, as well as with configurations and mutual coupling between the π-loops. π-loops with 3 μm or 6 μm wide ds-JJs demonstrated spontaneous fluxes of approximately $\Phi_0/2$, indicating that all of the investigated π-loops have the screening parameter $ß_L >> 1$. We manipulated the magnetic states of the π-loops by the local application of magnetic fields using integrated planar coils. Our work paves the way for the use of π-loops in computations based on Application Specific Annealing Computing (ASAC) [19], quantum annealing processes [20], an adiabatic superconducting artificial neural network [21], and/or in RSFQ circuits [22].

REFERENCES

[1] D. J. Van Harlingen, "Phase-sensitive tests of the symmetry of the pairing state in the high-temperature superconductors–Evidence for $d_{x^2-y^2}$ symmetry," *Rev. Modern Phys.*, vol. 67, pp. 515–535, 1995.

[2] H. Hilgenkamp *et al.*, "Ordering and manipulation of the magnetic moments in large-scale superconducting π-loop arrays," *Nature*, vol. 422, pp. 50–53, 2003.

[3] H. J. H. S. Ariando, D. H. A. B. H. Hilgenkamp, and H. Rogalla, "π-SQUIDs based on Josephson contacts between high-T_c and low-T_c superconductors," *Phys. Rev. B*, vol. 70, 2004, Art. no. 024519.

[4] L. B. Ioffe, V. B. Geshkenbein, M. V. Feigel'man, A. L. Fauchere, and G. Blatter, "Environmentally decoupled sds-wave Josephson junctions for quantum computing," *Nature*, vol. 398, pp. 679–681, 1999.

[5] T. Ortlepp *et al.*, "RSFQ circuitry using intrinsic π-phase shifts," *IEEE Trans. Appl. Supercond.*, vol. 17, no. 2, pp. 659–663, Jun. 2007.

[6] A. K. Feofanov *et al.*, "Implementation of superconductor/ferromagnet/superconductor π-shifters in superconducting digital and quantum circuits," *Nature Phys.*, vol. 6, pp. 593–597, 2010.

[7] S. V. Bakurskiy *et al.*, "Protected 0-π states in SIsFS junctions for Josephson memory and logic," *Appl. Phys. Lett.*, vol. 113, 2018, Art. no. 082602.

[8] S. Kawabata, A. A. Golubov, C. J. M. V. Ariando, H. Hilgenkamp, and J. R. Kirtley, "Macroscopic quantum tunneling and quasiparticle-tunneling blockade effect in s-wave/d-wave hybrid junctions," *Phys. Rev. B*, vol. 76, 2007, Art. no. 064505.

[9] A. Y. Tzalenchuk *et al.*, "Feasibility studies of ultra-small Josephson junctions for qubits," *IEEE Trans. Appl. Supercond.*, vol. 13, no. 2, pp. 948–951, Jun. 2003.

[10] M. I. Faley, S. B. Mi, A. Petraru, C. L. Jia, U. Poppe, and K. Urban, "Multilayer buffer for high-temperature superconductor devices on MgO," *Appl. Phys. Letters*, vol. 89, 2006, Art. no. 082507.

[11] J. R. Kirtley *et al.*, "High-resolution scanning SQUID microscope," *Appl. Phys. Letters*, vol. 66, 1995, Art. no. 1138.

[12] J. R. Kirtley and J. P. Wikswo, "Scanning SQUID microscopy," *Annu. Rev. Mater. Sci.*, vol. 29, pp. 117–148, 1999.

[13] P. Reith, X. Renshaw Wang, and H. Hilgenkamp, "Analysing magnetism using scanning SQUID microscopy," *Rev. Sci. Instrum.*, vol. 88, 2017, Art. no. 123706,

[14] U. Poppe *et al.*, "Low-resistivity epitaxial $YBa_2Cu_3O_{7-x}$ thin films with improved microstructure and reduced microwave losses," *J. Appl. Phys.*, vol. 71, 1992, Art. no. 5572.

[15] M. I. Faley and U. Poppe, Patent EP2630650 B1, Oct 5, 2016.

[16] M. I. Faley *et al.*, "High-T_c SQUID biomagnetometers," *Supercond. Sci. Technol.*, vol. 30, 2017, Art. no. 083001.

[17] M. M. Khapaev, M. Y. Kupriyanov, E. Goldobin, and M. Siegel, "Current distribution simulation for superconducting multi-layered structures," *Supercond. Sci. Technol.*, vol. 16, pp. 24–27, 2003.

[18] A. A. Golubov, M. Y. Kupriyanov, and E. Il'ichev, "The current-phase relation in Josephson junctions," *Rev. Modern Phys.*, vol. 76, pp. 411–469, 2004.

[19] S. Kawabata, "Large-scale superconducting quantum annealing machine based on 2.5D packaging technology and application specific architecture," *in Proc. Int. Sci. Conf. Supercond. Quantum Technol.*, Jul. 30–Aug. 3, 2018, pp. 20–21.

[20] P. I. Bunyk *et al.*, "Architectural considerations in the design of a superconducting quantum annealing processor," *IEEE Trans. Appl. Supercond.*, vol. 24, no. 4, Aug. 2014, Art. no. 1700110.

[21] I. I. Soloviev *et al.*, "Adiabatic superconducting artificial neural network: Basic cells," *J. Appl. Phys.*, vol. 124, 2018, Art. no. 152113.

[22] T. Ortlepp *et al.*, "Flip-flopping fractional flux quanta," *Science*, vol. 312, pp. 1495–1497, Jun. 9, 2006.